DEFECT IDENTIFICATION IN SILICON USING ELECTRON NUCLEAR DOUBLE RESONANCE

C.A.J. AMMERLAAN, M. SPRENGER, R. VAN KEMP AND D.A. VAN WEZEP
Natuurkundig Laboratorium der Universiteit van Amsterdam, Valckenierstraat 65, 1018 XE Amsterdam, The Netherlands

ABSTRACT

The application of electron nuclear double resonance (ENDOR) for identification and characterization of point defects in silicon is reviewed. Taking the vacancy and the boron-vacancy complex as examples it is discussed how ENDOR can provide information on the atomic and electronic structure of paramagnetic centers.

OUTLINE OF EXPERIMENTAL RESULTS

Electron Nuclear DOuble Resonance (ENDOR) is a spectroscopic technique which, in ideal cases , unites the high sensitivity of Electron Paramagnetic Resonance (EPR) and the high energy resolving power of Nuclear Magnetic Resonance (NMR). Its application requires the simultaneous presence of an electronic and a nuclear magnetic moment in the defect to be studied. It is useful to distinguish between self-ENDOR, in which a possible magnetic nucleus of a constituent impurity of the center participates, and ligand-ENDOR with the ^{29}Si nuclei (I=1/2) of the host crystal. Following its introduction by Feher in 1959 [1,2], ENDOR examinations have been made for about 30 centers in silicon, including the group V shallow donors, the chalcogen double donors, several of the 3d-transition metal impurities, and a number of irradiation-produced defects. Table I summarizes some of the relevant properties of these centers. In the next paragraphs of this paper a discussion will be given on the chemical nature of impurities forming the centers, and on their atomic and electronic size and shape, as determined by ENDOR.

INFORMATION ON CHEMICAL CONSTITUENTS

ENDOR spectra are most conveniently analyzed using a spin-Hamiltonian, such as

$$H = +\mu_B \vec{B}.\vec{g}_e.\vec{S} - g_n\mu_N \vec{B}.\vec{I} + \vec{S}.\vec{A}.\vec{I} + \sum_i (-g_{Si}\mu_N \vec{B}.\vec{I}_i + \vec{S}.\vec{A}_i.\vec{I}_i) \quad (1)$$

representing the electronic paramagnetic energy in the magnetic field $\vec{B}$, interactions with one magnetic impurity isotope, with nuclear spin I, and the interactions with several ^{29}Si isotopes, $I_{Si}=1/2$, on the sites i around the center. For isotropic centers in high field approximation the energies are given by

$$E = +g_e\mu_B B m_S - g_n\mu_N B m_I + a m_S m_I + \sum_i (-g_{Si}\mu_N B m_{Ii} + a_i m_S m_{Ii}) \quad (2)$$

The ENDOR transitions for the impurity follow from the selection rules $\Delta m_S=0$, $\Delta m_I=\mp 1$, $\Delta m_{Ii}=0$:

$$h\nu = |g_n\mu_N B - a m_S| \quad (3)$$

Likewise, the ^{29}Si ligand-ENDOR frequencies ν_i are

$$h\nu_i = |g_{Si}\mu_N B - a_i m_S| \quad (4)$$

An energy level scheme applicable to the boron-vacancy-complex in silicon,

Mat. Res. Soc. Symp. Proc. Vol. 46. © 1985 Materials Research Society

Table I. Summary of ENDOR studies of centers in silicon. V^* is chemical symbol for vanadium; all other characters V denote lattice monovacancy.

Center	EPR-spectrum	Spin	Symmetry	Self-ENDOR isotope	spin	Ligand-ENDOR shells	atoms	Reference
P		1/2	Cubic	^{31}P	1/2	5	30	1,2
				^{32}P	1			3
						23	216	5
As		1/2	Cubic	^{75}As	3/2	5	30	2
						22	204	5
Sb		1/2	Cubic	^{121}Sb	5/2	5	30	2,4
				^{123}Sb	7/2			
						17	166	5
Li			Cubic	^{6}Li	1		30	6
				^{7}Li	3/2			
S^+		1/2	Cubic	^{33}S	3/2	8	58	7
Se^+		1/2	Cubic			8	66	8
Te^+		1/2	Cubic			12	108	9
Ti^+	NL29	3/2	Cubic	^{47}Ti	5/2	17	214	10
$(V^*)^{++}$		3/2	Cubic	^{51}V	7/2			11
Cr^+		5/2	Cubic	^{53}Cr	3/2			11
Mn^-		1	Cubic	^{55}Mn	5/2			11
Mn^{++}		5/2	Cubic	^{55}Mn	5/2			11
Fe		1	Cubic	^{57}Fe	1/2			12
						6	42	13
Fe^+		1/2	Cubic	^{57}Fe	1/2			12
FeGa		1/2	Trigonal	^{57}Fe	1/2			12
CrAu		3/2	Trigonal	^{197}Au	3/2			14,15
$(MnAu)^+$		3/2	Trigonal	^{197}Au	3/2			14,15
$(MnAu)^-$		5/2	Trigonal	^{197}Au	3/2			14,15
PV	G8	1/2	Monoclinic I	^{31}P	1/2			16
AlV	G9	1	Trigonal	^{27}Al	5/2			17
AsV	G23	1	Monoclinic I	^{75}As	3/2			18
SbV	G24	1/2	Monoclinic I	^{121}Sb	5/2			18
Al_I^{++}	G18	1/2	Cubic	^{27}Al	5/2	1	4	19
B_i	G28	1/2	Monoclinic I	^{11}B	3/2			20
VV^+	G6	1/2	Monoclinic I			18	60	21
VV^-	G7	1/2	Monoclinic I			33	106	22
V^-	G2	1/2	Rhombic I			51	152	23
BV	G10	1/2	Triclinic	^{10}B	3	8	8	24
				^{11}B	3/2			
OV^-	B1	1/2	Rhombic I			50	145	25

with S=1/2 and I=3/2 for the ^{11}B isotope, is shown in figure 1, with EPR and ENDOR (=NMR) transitions indicated. Figure 2 is the corresponding ENDOR spectrum of six resonances, which consists of two groups of three lines each. The three lines above the nuclear Zeeman frequency $g_n\mu_N B$ are separated from the three lines below by the hyperfine interaction; the structure within the groups is due to nuclear quadrupole effects [24]. From straightforward analysis of such spectra both the nuclear spin value I and the nuclear moment follow, thus providing unambiguous identification of the impurity and/or ^{29}Si nucleus. In the example given, the hyperfine interactions are too small to be resolvable in EPR [26]; as shown the enhanced resolution of ENDOR is quite sufficient. Expression (1) is not necessarily entirely adequate for analysis of the spectra. In the case of higher spin it may be necessary to include quadrupole interaction, such as for Si:BV (see

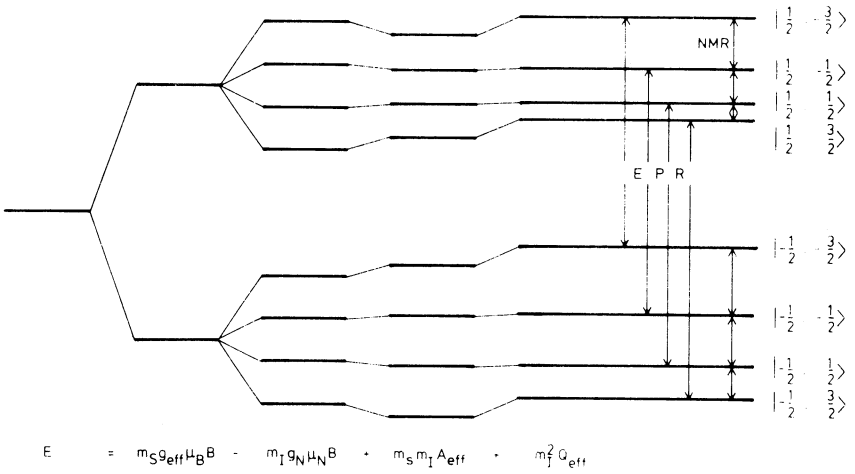

Figure 1. Level scheme for Si:BV, with S=1/2 and I=3/2 for the ^{11}B isotope. EPR and NMR (=ENDOR) transitions are indicated.

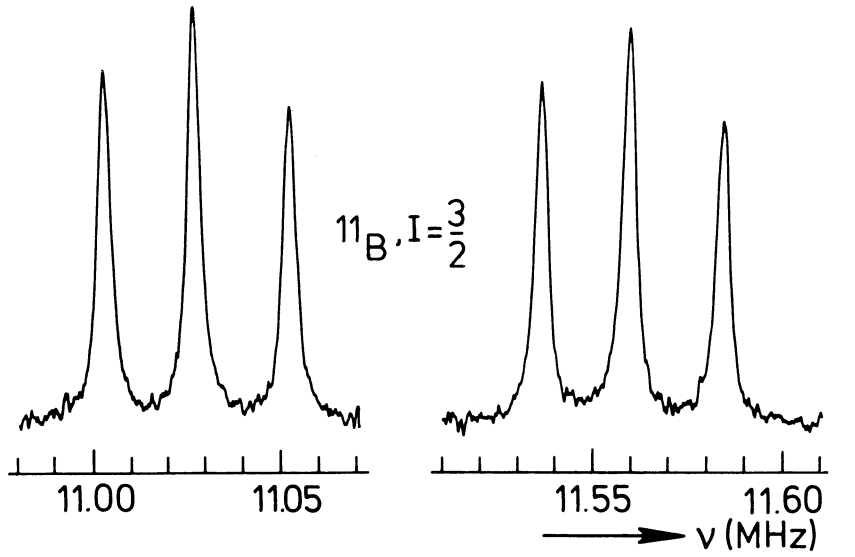

Figure 2. ENDOR spectra of Si:BV. The highest-field EPR transition of the Si-G10 spectrum was saturated with magnetic field parallel to [100] and equal to 826.73 mT; microwave frequency 23.176 GHz.

figures 1 and 2), or higher order hyperfine terms, e.g. in the case of $Si:Ti^+$. These additional interactions allow further characterization of the center.

INFORMATION ON SHAPE

The point-group is the crystallographic characterization of the shape of any defect. For single impurities on substitutional sites all symmetry elements of the silicon crystal are retained in the fine-structure as observed in EPR and the point-group is the cubic $\bar{4}3m$. As table I shows, examples are abundant. A defect of complex structure may destroy all symmetry elements of the host, which results in the lowest-possible triclinic symmetry. There are few examples of this situation: Si-G10, associated with the boron-vacancy complex Si:BV and iron-related spectrum Si-NL23 are the only ones known so far. According to this point of view a symmetry classification distinguishing eight different cases can be made. Coincidences in the resonance positions, as resulting from the orientational degeneracy, are revealed in the angular patterns and unambiguously determine the crystallographic system. Table II summarizes these symmetry aspects.

When studying ligand hyperfine interactions the combined symmetry of defect plus ^{29}Si nucleus is relevant. For a highest symmetry site of the ^{29}Si this may be the holohedral point-group of the defect; such sites do not always exist and in general it will be a subgroup. With ENDOR, hyperfine interactions with ligand ^{29}Si nuclei were determined in detail for several centers. The negative lattice vacancy, $Si:V^-$, which has rhombic I, point-group 2mm symmetry, may serve as an example. Depending on the ^{29}Si position with respect to the two inequivalent mirrorplanes of the vacancy, the symmetry will remain rhombic I, or will be lowered to monoclinic I or triclinic. Figure 3 illustrates this behavior. With ENDOR the symmetry classification of a center, usually already known from EPR, can be confirmed. The excellent resolution and the availability of many shells of hyperfine atoms eliminates the risk of accidental degeneracies.

Table II. Symmetry classification of centers in silicon.

System	Point-group(s)	Resonances in direction <100>	<111>	<011>
Cubic	$\bar{4}3m$,23	1	1	1
Tetragonal	$\bar{4}2m$,$\bar{4}$	2	1	2
Rhombic I	2mm	2	2	3
Rhombic II	222	3	1	3
Trigonal	3m,3,$\bar{3}$m,$\bar{3}$	1	2	2
Monoclinic I	2/m,m	2	3	4
Monoclinic II	2	3	2	4
Triclinic	1,$\bar{1}$	3	4	6

INFORMATION ON ELECTRONIC SIZE

The isotropic part of the hyperfine interaction arises from the contact interaction. It is related to the s-part of the defect's electron wavefunction at position r_i by

$$a = (\mu_o/4\pi)(8\pi/3)g_e\mu_B g_n\mu_N|\psi(r_i)|^2 \qquad (5)$$

Assuming, although no general proof is available , a monotonic decrease of the wavefunction with distance to the center within symmetry classes, an ordered density distribution $|\psi(r_i)|^2$ of the defect electron is obtained. Data for the negative vacancy in silicon are presented in figure 4a, together with an empirical fit of these data by the exponential relation

$$\psi^2 = A^2\exp(-2r/r_o) \qquad (6)$$

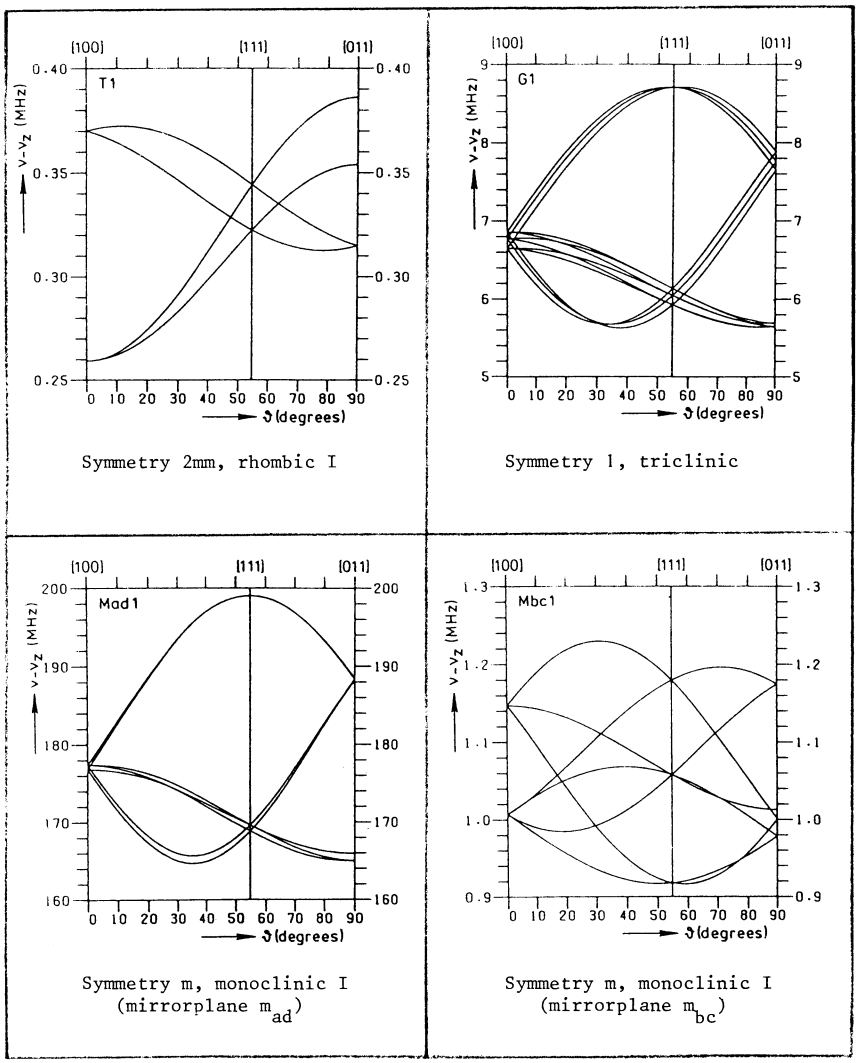

Figure 3. Angular dependence of the ENDOR frequencies for the triclinic, monoclinic I and rhombic I class shells of the negative vacancy in silicon.

The pre-exponential density parameter A^2 and the characteristic decay length r_o for the match as shown are given in table 3, which also contains the results of the corresponding analysis for the divacancy in positive and negative charge states. For these typical deep level defects the characteristic electronic range is near 2 to 3.10^{-10} m. This figure gains perspective by comparing with the value 15 to 20.10^{-10} m which the effective mass theory predicts for shallow donor levels. The inequivalence of the two mirrorplanes is clearly demonstrated in the strong preference of the plane

labelled m_{ad}, which has A^2=10, over the plane m_{bc} with A^2=0.1. Rather than being isotropically distributed, the vacancy electron is concentrated in one plane. Also on an empirical basis the plot as presented in figure 4b was made. It was noted that several of the hyperfine tensors in the Mad class have a very similar structure, suggesting a direct and simple relation between them. A plot of the isotropic part of these tensors as a function of distance to the vacancy along a [011] chain results in nearly perfect exponential decay. The characteristic range $4.7.10^{-10}$ m indicates a markedly enhanced extension in this particular direction [23].

Table III. Parameters describing the wavefunctions of the vacancy and divacancy in silicon.

Defect	Class	A^2 (10^{-24} cm^{-3})	r_o
V^-	Mad	10	2.4
	Mbc	0.1	3.0
	G	0.6	3.2
V^-	Mad	3.3	4.7
VV^-	M	2	3.0
	G	1.1	2.6
VV^+	M	7	1.9
	G	4.3	1.9

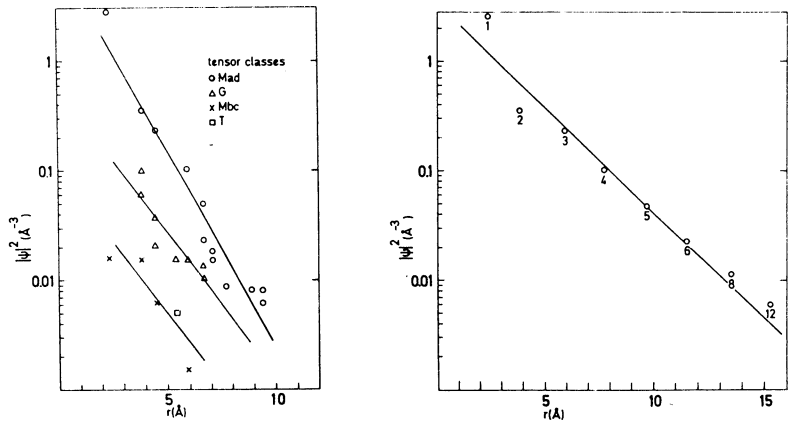

(a) (b)

Figure 4. Probability density for the wavefunction of the negative vacancy as a function of distance to the vacant site, (a) for ordering within each symmetry class, (b) with preferential ordering along a [011] chain for specific tensors in the Mad class, as discussed in reference 23.

INFORMATION ON ELECTRONIC STRUCTURE

The analysis of the hyperfine interactions for Si:V^- indicated a very small spin density in the mirrorplane m_{bc}. This result is to be interpreted as a virtually vanishing spin density, a situation which then slightly is perturbed, as will be discussed. A zero value for the s-part of the spin density on the mirrorplane m_{bc} implies odd symmetry, character -1, for reflection with respect to this plane. Even symmetry, character +1, for mirrorplane m_{ad} is implied by the strong contact interaction with ^{29}Si nuclei in this plane. Only the irreducible representation b_1 of point-group 2mm is consistent with these requirements. From ligand-ENDOR the symmetry-type of the wavefuction can be deduced in this way. For the present example of Si:V^- the conclusion agrees with the electronic model which constructs a defect wavefunction as an LCAO of the sp^3-hybridized dangling bonds a, b, c and d on the four nearest-neighbors of the vacancy [27]. Figure 5 illustrates the occupation of levels and orbitals by the 5 electrons of the negative vacancy.

An explanation of the small non-vanishing a-value can be found in a many-electron description. The 5-electron ground state as illustrated in figure 5 is given by the wavefunction $\psi_o=|a_1\bar{a}_1a_1''\bar{a}_1''b_1\rangle$, with symmetry-label $^2B_1$. Excited states with the same symmetry are $\psi_1=|a_1\bar{a}_1b_1b_2\bar{b}_2\rangle$, $\psi_2=|a_1''\bar{a}_1''b_1b_2\bar{b}_2\rangle$, $\psi_3=|a_1\bar{a}_1''b_1b_2\bar{b}_2\rangle$ and $\psi_4=|a_1''\bar{a}_1b_1b_2\bar{b}_2\rangle$. In an improved description of the defect electrons these excited states will be admixed into ψ_o. The configurations ψ_3 and ψ_4 have a non-zero spin density on the bc-plane, as the spin of the electron in the a_1 orbital will not be cancelled by the opposite spin in the a_1'' orbital. Exchange interactions are responsible for unequal admixture of the ψ_3 and ψ_4 excited states. Although a theoretical estimate of this polarization phenomenon has produced good agreement [28], much of the quantitative understanding is still to be achieved .

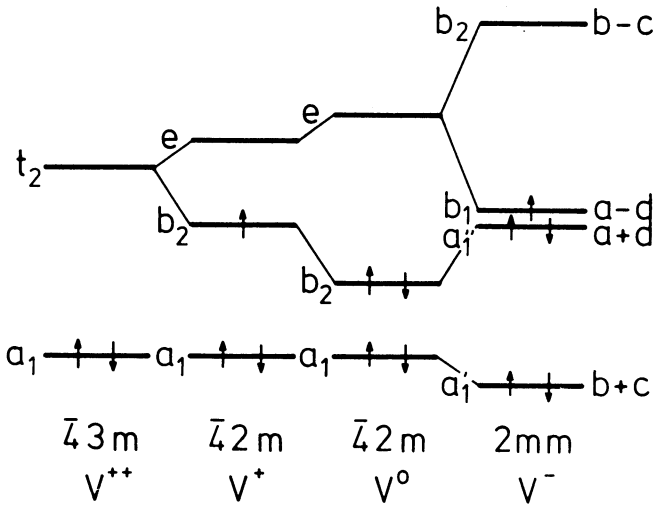

Figure 5. LCAO level scheme of the vacancy in silicon for various charge states, after Watkins [27].

INFORMATION ON ATOMIC STRUCTURE

So far, only the isotropic part of the hyperfine tensors has been considered. However, for the traceless anisotropic part, a more ready interpretation in terms of dipole-dipole interaction between the electronic and nuclear magnetic moments is sometimes applicable. As an illustration the Si:BV-complex is considered. The hyperfine tensor $\overleftrightarrow{A}$ as measured for the interaction with the boron impurity in the complex is decomposed into scalar part a and dipolar part $\overleftrightarrow{B}$ by $\overleftrightarrow{A}=a\overleftrightarrow{1}+\overleftrightarrow{B}$. Table IV gives the relevant numerical values. It is observed that tensor $\overleftrightarrow{B}$ is nearly axial, and may be approximated by an axial tensor with principal values (B_1,B_2,B_3) = (+690kHz, -345kHz,-345kHz). Such an interaction tensor is consistent with a distant dipole-dipole interaction, which is easily calculated in a point-dipole approximation. From the ENDOR data the electronic spin distribution is already known in some detail, e.g. in this case about 55% of the unpaired electron is localized on the dangling bond on atom a in figure 6. The axial direction of tensor $\overleftrightarrow{B}$, given by the direction cosines [-0.792,-0.609, +0.038], coincides with the orientation of the position vector of the boron atom; the magnitude of the principal values is related to the distance between the nuclear moment and the electronic center. On the basis of these arguments the two most probable boron lattice sites are B and B', as indicated in figure 6. Between the two sites, which are in opposite direction as seen from the vacancy in the origin, no distinction can be made. The hyperfine tensor constants calculated for the sites B are included in table IV. They are considered to be in good agreement with the measured values.

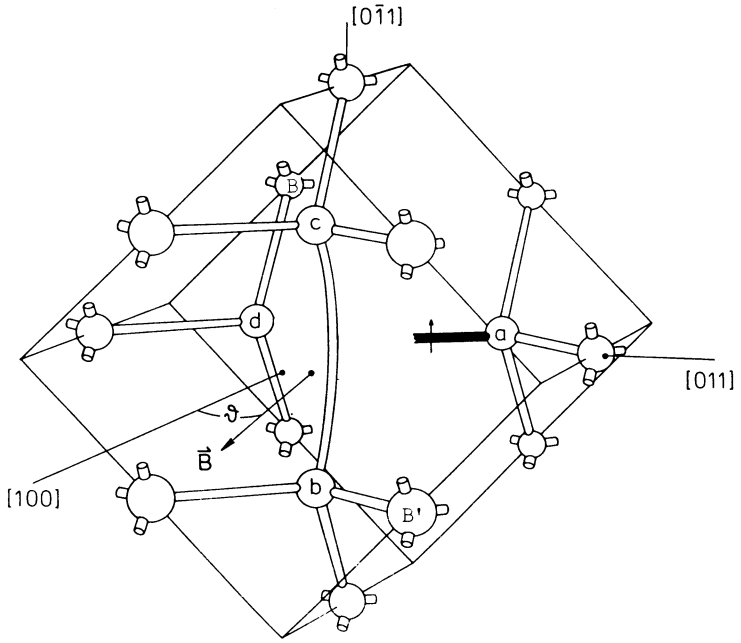

Figure 6. Atomic model, not showing all distortions, for the boron-vacancy complex in silicon. Probable positions for the boron atom are marked B and B'.

Table IV. Hyperfine parameters for the B-atom, isotope ^{11}B, in the boron-vacancy complex, after Sprenger et al [24].

i	A_i (kHz)	Direction cosines n[100]	n[010]	n[001]	a (kHz)	$B_{i,exp}$ (kHz)	$B_{i,calc}$ (kHz)
1	+537	-0.792	-0.609	+0.038	-154	+691	+491
2	-459	-0.584	+0.774	+0.243		-305	-246
3	-541	-0.177	+0.170	-0.969		-387	-246

SUMMARY

The elucidation of the atomic and electronic structure of point defects in silicon by ENDOR was discussed, with illustrative arguments taken from studies of the negative lattice vacancy and the boron-vacancy complex. It was shown that from ENDOR an identification of the impurities in the center is obtained, the point-group symmetry of the defect is established, and the symmetry-type of the wavefunction is determined. In addition the characteristic range of the defect electron is measured with sometimes very detailed information on the angular distribution. Atomic coordinates as derived from ENDOR data may assist in postulating specific atomic models.

References

1. G. Feher, Phys. Rev. 103,834(1956).
2. G. Feher, Phys. Rev. 114,1219(1959).
3. G. Feher, C.S. Fuller and E.A. Gere, Phys. Rev. 107,1462(1957).
4. J. Eisinger and G. Feher, Phys. Rev. 109,1172(1958).
5. E.B. Hale and R.L. Mieher, Phys. Rev. 184,739(1969).
6. G.D. Watkins and F.S. Ham, Phys. Rev. B1,4071(1970).
7. G.W. Ludwig, Phys. Rev. 137,A1520(1965).
8. S. Greulich-Weber, J.R. Niklas and J.-M. Spaeth, J. Phys. C: Solid State Phys. 17,L911(1984).
9. J.R. Niklas and J.-M. Spaeth, Solid State Comm. 46,121(1983).
10. D.A. van Wezep and C.A.J. Ammerlaan, J. Electron. Mat. 14a,863(1985), and to be published.
11. H.H. Woodbury and G.W. Ludwig, Phys. Rev. 117,102(1960).
12. G.W. Ludwig and H.H. Woodbury, Phys. Rev. 117,1286(1960).
13. S. Greulich-Weber, J.R. Niklas, E.R. Weber and J.-M. Spaeth, Phys. Rev. B30,6292(1984).
14. H.H. Woodbury and G.W. Ludwig, Phys. Rev. 117,1287(1960).
15. G.W. Ludwig and H.H. Woodbury, Solid State Phys. 13,223(1962).
16. G.D. Watkins and J.W. Corbett, Phys. Rev. 134,A1359(1964).
17. G.D. Watkins, Phys. Rev. 155,802(1967).
18. E.L. Elkin and G.D. Watkins, Phys. Rev. 174,881(1968).
19. K.L. Brower, Phys. Rev. B1,1908(1970).
20. G.D. Watkins, Phys. Rev. B12,5824(1975).
21. J.G. de Wit, E.G. Sieverts and C.A.J. Ammerlaan, Phys. Rev. B14,3494 (1976).
22. E.G. Sieverts, S.H. Muller and C.A.J. Ammerlaan, Phys. Rev. B18,6834 (1978).
23. M. Sprenger, S.H. Muller and C.A.J. Ammerlaan, Physica 116B,224(1983).
24. M. Sprenger, R. van Kemp, E.G. Sieverts and C.A.J. Ammerlaan, J. Electron. Mat. 14a,815(1985).
25. R. van Kemp, E.G. Sieverts, M. Sprenger and C.A.J. Ammerlaan, to be published.
26. G.D. Watkins, Phys. Rev. B13,2511(1976).
27. G.D. Watkins, Inst. Phys. Conf. Series 16,228(1973).
28. M. Lannoo, Phys. Rev. B28,2403(1983).